SUPPORTING INFORMATION

Representation of Activities of Electrocatalysts for Water Oxidation Dynamic Potential/pH Diagrams

Alessandro Minguzzi[a], Fu-Ren F. Fan[b], Alberto Vertova[a], Sandra Rondinini[a] and Allen J. Bard[b]

[a]*Dipartimento di Chimica Fisica ed Elettrochimica, Universitá degli Studi di Milano, Via Golgi, 19, 20133, Milan, Italy*

[b]*Center for Electrochemistry, Department of Chemistry and Biochemistry, The University of Texas at Austin, Austin, TX 78712-0165*

Experimental

Cyclic voltammetry

All cyclic voltammograms were recorded using a saturated Ag/AgCl and a Pt coil (or a graphite rod) as the reference and the counter electrode, respectively. The reference electrode was inserted in a pipette filled with agar impregnated with 0.2 M $NaClO_4$. All measurements were conducted using a CH Instrument 920c scanning electrochemical microscope bipotentiostat, varying the scan rate between 400 and 2 mV/s. Electrolyte solutions were bubbled with Ar prior to every measurement. Each material was tested at at least three different pH values. IrO_2 and Pt were characterized in 1 M $HClO_4$ (pH 0.1), 1 M phosphate buffer solution (PBS, pH 6.8, obtained by an equimolar mixture of NaH_2PO_4 and Na_2HPO_4) and 1 M NaOH (pH 14.0). Neutral pH conditions were achieved also using 1 M $NaClO_4$ (pH 6.0) to study the effect of unbuffered solutions.

Cobalt-based materials are unstable in acidic media, therefore they were studied in acetate buffer solution (pH 4.7, obtained by mixing equimolar solutions of acetic acid and sodium acetate), 1 M PBS at pH 6.8 (obtained by an equimolar mixture of NaH_2PO_4 and Na_2HPO_4) and pH 11.3 (obtained by an equimolar mixture of Na_3PO_4 and Na_2HPO_4), as well as in 1 M NaOH. All electrolyte solutions were prepared by using deionized Milli-Q water. $HClO_4$, NaOH, Na_3PO_4, Na_2HPO_4, NaH_2PO_4), acetic acid and sodium acetate were reagent grade and were used as received.

The integration of CV areas was performed by using the CHI 920c SECM software on the anodic half-scan on the second recorded cycle. For the IrO_2 electrode, the integration was done over

a potential window 0.4 to 1.3 V (vs. RHE) while for Co_3O_4 only the main peak prior to the OER was considered.

Determination of the number of active sites in oxide electrocatalysts

The purpose of this supporting paragraph is to describe the method adopted to determine the number of active sites and the theory behind it.

As discussed in the main text, the best estimate of the real surface area of oxide electrocatalysts is related to the number of sites involved in surface (pseudocapacitive) reactions like:

$$MO_x(OH)_y + \delta H^+(solution) + \delta e^-(oxide) \rightarrow MO_{x-\delta}(OH)_{y+\delta} \quad (1)$$

which are accompanied by the usual contributions of double layer capacitance charge/discharge processes. Capacitance and pseudocapacitance features are clearly visible in the cyclic voltammograms (CVs) of both IrO_2 and Co_3O_4. Peaks due to pseudocapacitive phenomena overlap contributions from other phenomena (see the following text).

CVs of IrO_2 in acidic or alkaline pHs clearly show two main peaks, usually associated with Ir(III)-Ir(IV) and Ir(IV)-Ir(V) transitions.[1,2,3] The marked difference between acid and alkaline characteristics is probably due to the initial surface state and to the nature of the species involved in the reaction. We suggest that in this case reaction 1 can be rewritten as (Scheme 1):

Scheme 1

$$\begin{array}{ccccc}
MO_xO^-_y + \delta H_2O + \delta e^- & \rightleftarrows & MO_{x-\delta}(OH)_\delta O^-_y + \delta \mathbf{OH}^- & \rightleftarrows & MO_{x-\delta}O^-_{y+\delta} + \delta H_2O \\
\updownarrow \pm yH^+ & & & & \updownarrow \pm(y+\delta)H^+ \\
MO_x(OH)_y + \delta \mathbf{H}^+ + \delta e^- & \rightleftarrows & & & MO_{x-\delta}(OH)_{y+\delta} \\
\updownarrow \pm yH^+ & & & & \updownarrow \pm(y+\delta)H^+ \\
MO_x(OH_2^+)_y + \delta \mathbf{H}^+ + \delta e^- & \rightleftarrows & MO_{x-\delta}(OH)_\delta(OH_2^+)_y & \overset{\pm\delta H^+}{\rightleftarrows} & MO_{x-\delta}(OH_2^+)_{y+\delta}
\end{array} \quad (2)$$

which takes into account the acid/base equilibria occurring at the oxide surfaces in aqueous solutions and displays well the processes occurring during the voltammetric scans at different pHs. This picture reflects the behavior of IrO_2 electrodes, as represented in Figure S1.

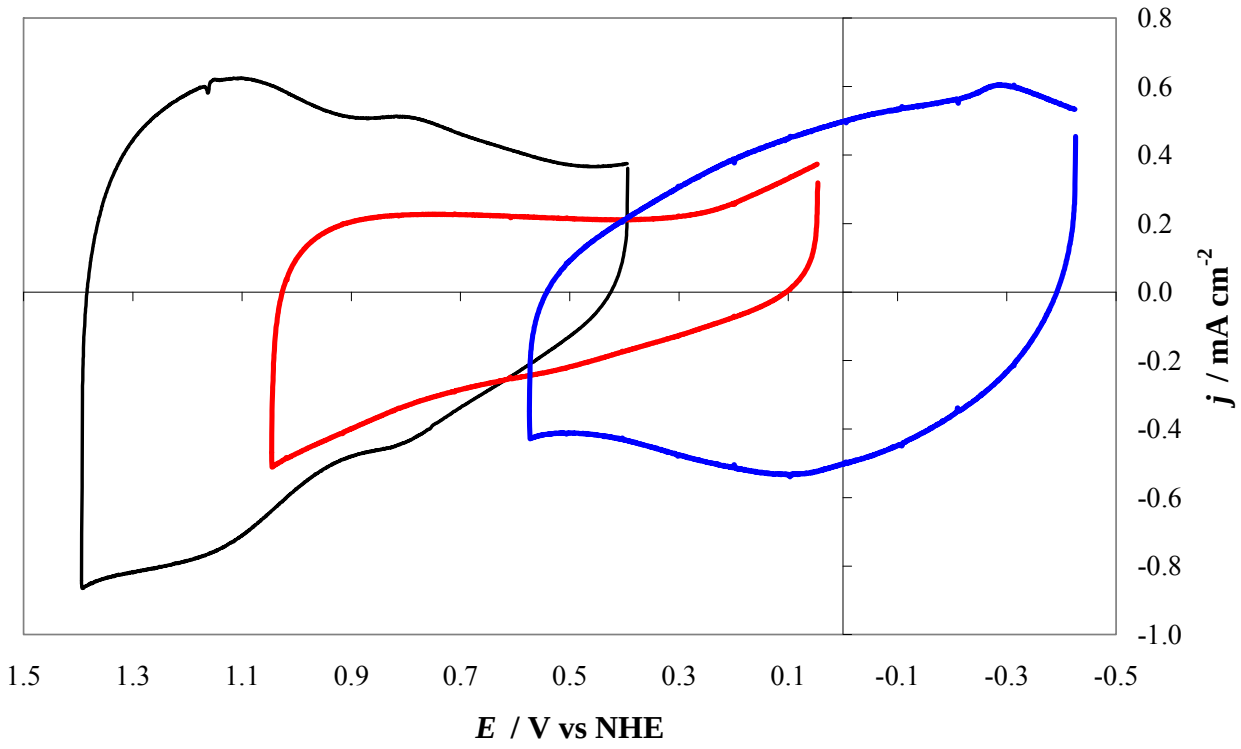

Figure S1. Cyclic voltammograms of an IrO_2 electrode (prepared by thermal decomposition of a $IrCl_3$ solution at 500°C) in 1 M $HClO_4$, (pH 0.1, black curve), 1 M $NaClO_4$ at (pH 6.0, red curve) and 1 M NaOH (pH 14, blue curve). Scan rate: 100 mV s^{-1}.

The larger amount of charge accumulated in strongly acidic and alkaline media is due to the abundance of H^+ or OH^-, which are included in the equilibria reported in Scheme 1.
In neutral media (central line in Scheme 1), the low concentration of H^+ ions leads to a lower quantity of accumulated charge. CVs recorded in the presence of $NaClO_4$ are mainly generated by double layer capacitance but also show, at the two extremes of the potential windows, characteristics due to pseudocapacitive reactions, e.g., at about 0.1 V (vs. NHE) in the cathodic scan and 0.9 V in the anodic one. The shift of these characteristics in unbuffered, neutral solution is probably caused by surface pH changes associated with the pseudocapacitive processes. During the anodic scan, reaction 1 goes toward the left side, thus producing H^+ ions and decreasing the local pH, which shifts the equilibrium potential of the reaction toward more positive potentials. The opposite happens during the cathodic scan: H^+ ions are consumed, thus increasing the surface pH

and shifting the equilibrium potential toward less positive potentials. In other words, in unbuffered neutral media, pseudocapacitive processes are self-inhibiting. This hypothesis is confirmed by using concentrated phosphate buffer as supporting electrolyte, as shown in Figure S2. In fact, the voltammogram recorded in 1 M PBS is similar to the one recorded in 1 M $HClO_4$.

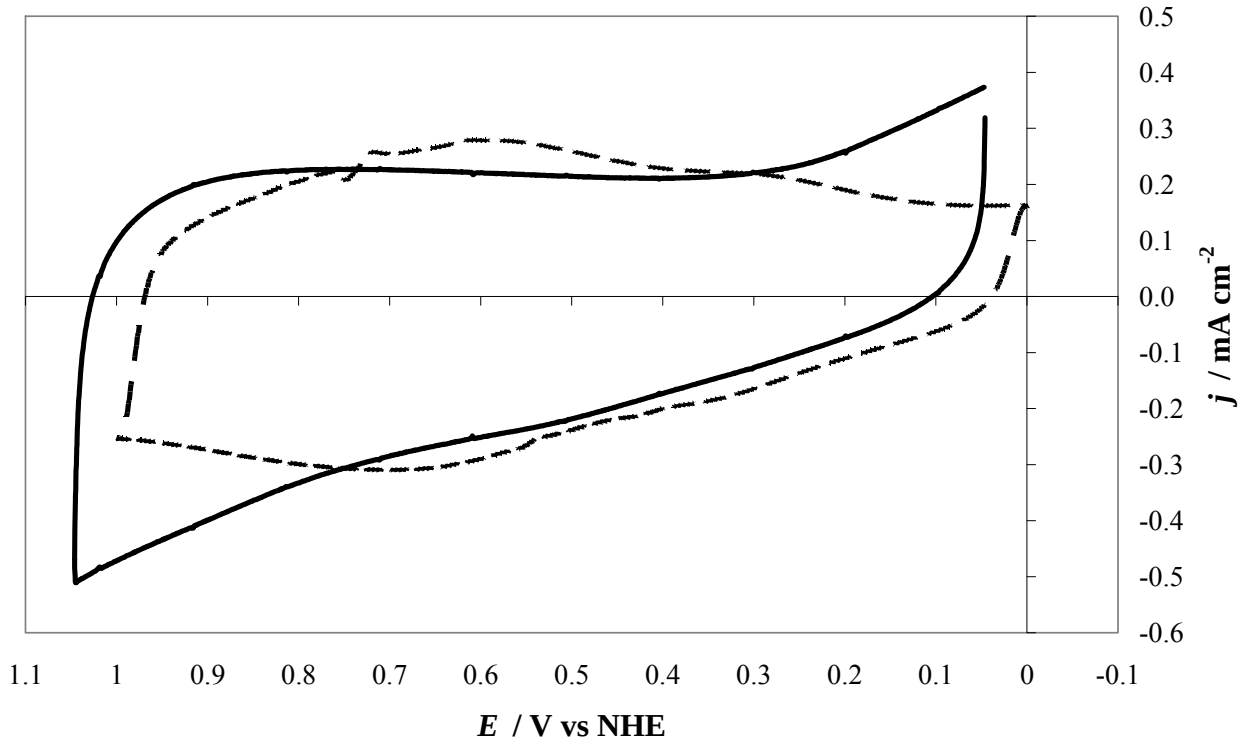

Figure S2. Cyclic voltammograms of an IrO_2 electrode (prepared by thermal decomposition of an $IrCl_3$ solution at 500°C) in 1 M PBS at (pH 6.8, dashed curve) and 1 M $NaClO_4$ (pH 6.0, continuous curve). Scan rate 100 mV s^{-1}.

The case of Co_3O_4 is analogous. An example of a CV recorded in neutral media is reported in Figure S3. The main pseudocapacitive phenomena are associated with the peak couple just before the large current increase from oxygen evolution at about 1.2 V (RHE). As suggested by other authors,[4,5] reaction 1 can be, in this case, translated into the following equation:

$$CoO_2 + H^+ + e^- \rightarrow CoOOH \text{ (the “hydrated form” of } Co_2O_3) \quad (3)$$

which is equivalent to the couple

$$2CoO_2 + 2\,H^+ + 2\,e^- \rightarrow Co_2O_3 + H_2O \quad (4)$$

with a standard potential, according to Pourbaix diagrams,[6] of 1.477 V vs RHE.

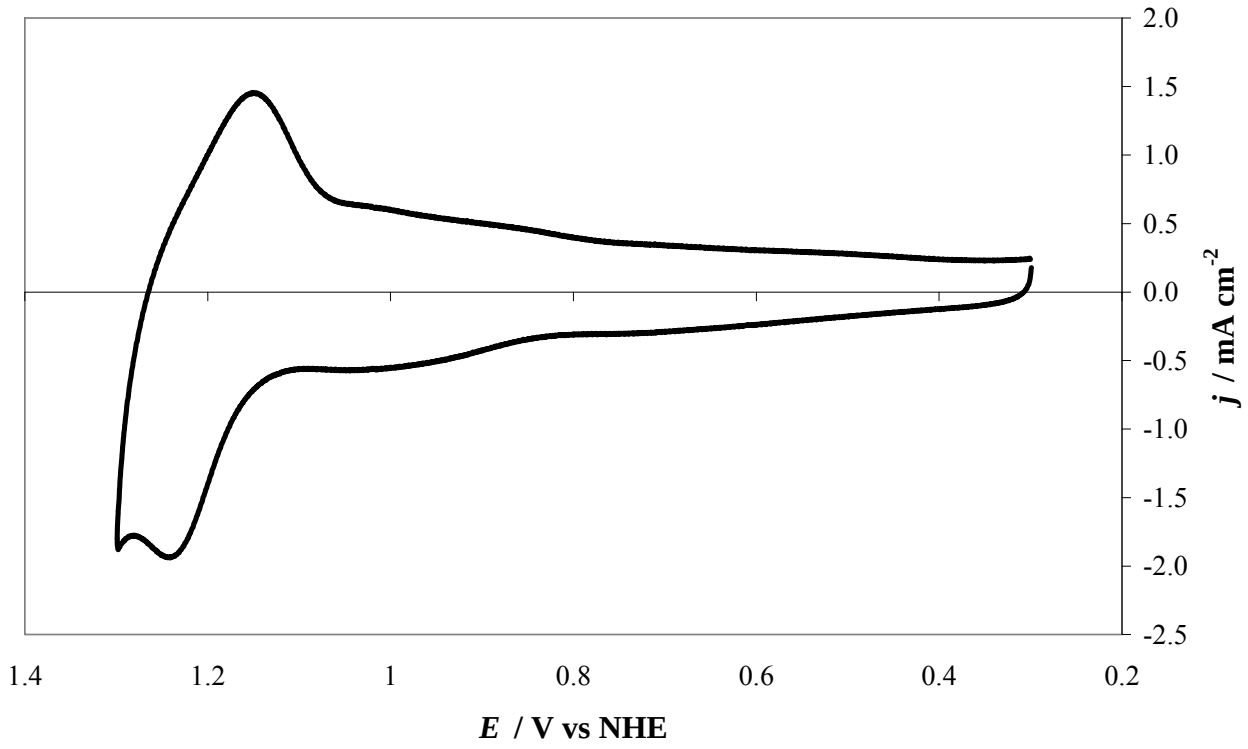

Figure S3. Cyclic voltammograms of a Co_3O_4 electrode (prepared by thermal decomposition of a $Co(NO_3)_2$ solution at 300°C) in 1 M PBS at (pH 6.8). Scan rate: 100 mV s^{-1}.

The other peak pairs observed at less positive potential are possibly related to steady state processes like:[4,5]

$$3CoOOH + H^+ + e^- \rightarrow Co_3O_4 + H_2O \quad (5)$$

and

$$Co_3O_4 + 2H_2O + 2H^+ + 2e^- \rightarrow 3Co(OH)_2 \text{ (a “hydrated form” of CoO)} \quad (6)$$

In the case of Co_3O_4, only the main peaks (associated with reaction 3) were taken into account for the estimation of the active area. However, for both materials, this is difficult, because pseudocapacitive phenomena are in principle indistinguishable from other contributions. The most

promising path is the use of scan rate for enhancing different phenomena. A possible solution is achievable by recording voltammograms at a very high scan rate, thus enhancing the double layer capacitance contribution, and subtracting it from the overall voltammetric characteristics. Unfortunately, pseudocapacitive characteristics are still visible at relatively high scan rates (up to a few V s^{-1}). At higher rates, uncompensated resistance distorts the signal. The second possible approach was proposed by Ardizzone *et al.*[7] who, after the first observations of proton diffusion in RuO_2 by Gerischer,[8] proved that the quantity of charge relevant to the voltammetric area in potential windows in which reaction 1 occurs depends on $v^{-1/2}$, where ν is the potential scan rate. This dependence was then observed on Co_3O_4[9] and IrO_2.[10]

An example of dependence of *Q* (in this case obtained by integration of the anodic scan of the second cycle of each CV) on the potential scan rate is given in Figure S4:

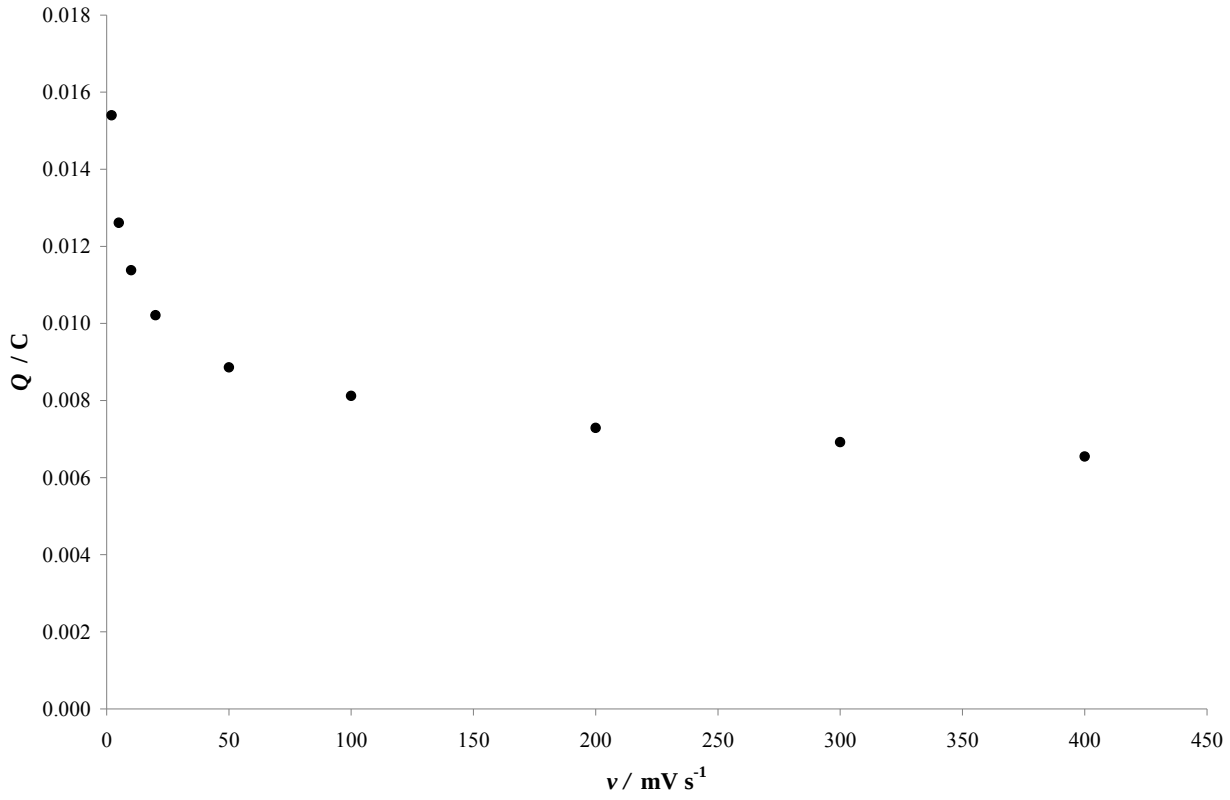

Figure S4. Quantities of charge (determined by integrating the anodic voltammetric curves between 0.4 and 1.3 V vs. RHE) accumulated by an IrO_2 electrode in 1 M $HClO_4$ (pH 0.1) as a function of the potential scan rate.

As discussed by Fierro et al.,[11] two explanations have been given for this behavior. The first originally proposed for RuO_2,[7] relates the dependence of *Q* to proton diffusion inside the porous oxide matrix. At high scan rates only the most "accessible" sites are involved in the charging

process, while at low scan rates the "poorly accessible" sites are also reached by the diffusing protons.

More recently two other phenomena were considered in detail for RuO_2 supported on glassy carbon: 1) double layer charging (and its related capacitance, which is independent of v) and 2) adsorption/desorption of the electrolyte ions, which determines the variation of capacitance inversely proportional to the potential scan rate.[12] In our opinion, the two points of view can be unified:[13] the double layer capacitance (whose contribution has been quantified by Fierro et al.[11]) is bound to the particle surface charging and can be considered as independent of scan rate; thus its contribution is embedded into the fraction of the most accessible sites. Pseudocapacitive, i.e. faradaic surface phenomena, account for both fast and slow charge storage sites, depending on the proton diffusion hindrance, which in turn depends on the material morphology and phase composition.

In more analytical terms, considering the total current is the sum of the capacitive and pseudocapacitive (i.e. faradaic, under H^+ diffusion control) contributions, the exchanged quantity of charge can be calculated as:

$$Q = \int_{E_1}^{E_2} \frac{I}{\upsilon} dE = \int_{E_1}^{E_2} \frac{C\upsilon + k\upsilon^{1/2}}{\upsilon} dE = C\left(E_2 - E_1\right) + \int_{E_1}^{E_2} \frac{k}{\upsilon^{1/2}} dE = C\left(E_2 - E_1\right) + \frac{k}{\upsilon^{1/2}}\left(E_2 - E_1\right) \qquad (7)$$

Obviously, equation 7 is an approximation since it doesn't take into account both the presence of any specific adsorbing ion and a possible dependence of C on the scan rate.

The incompleteness of the equation is proved by the fact that, for null scan rate, it would give an infinite accumulated charge. Notwithstanding the incompleteness of the model, Q can be further manipulated to obtain the separate contributions, Q_{out} and Q_{in}, which are the "outer" quantity of charge, Q_{out}, related to the number of the more accessible sites and the "inner" quantity of charge, Q_{in}, related to the less accessible sites. The estimation of Q_{out} is obtained by the linearization of equation 3, thus plotting Q vs $\nu^{1/2}$ and extrapolating $\nu^{-1/2} \rightarrow 0$ (corresponding to the extrapolation to infinite scan rate, See Figure S5).

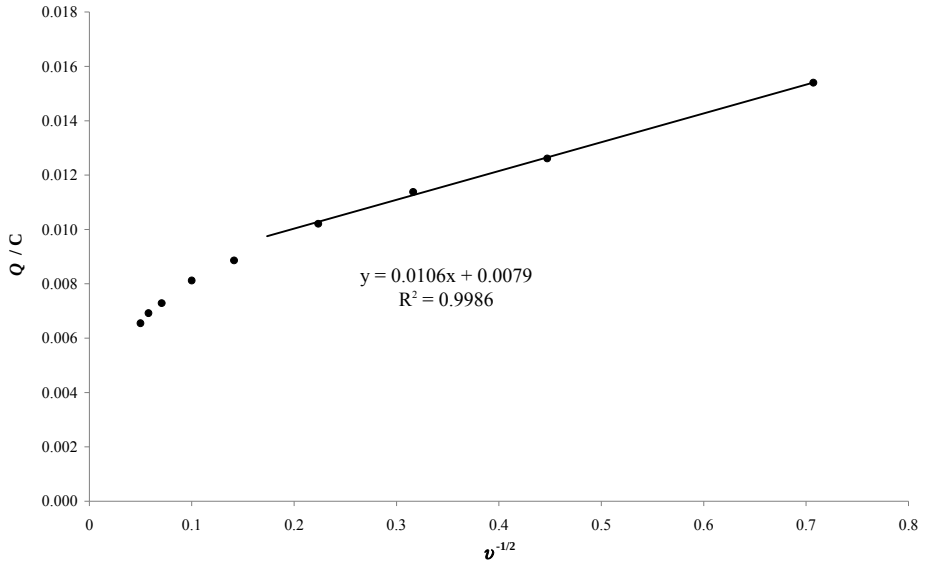

Figure S5. An example of extrapolation of Q to $v \rightarrow \infty$, on the data represented in Figure S4, for the determination of Q_{out}.

Due to the approximate nature of the analytical form of equation 3, the extrapolation of Q to $v \rightarrow 0$, as with the method proposed,[7] can easily cause unreliable results. The same is true for the extrapolation for $v^{1/2} \rightarrow 0$, of the $1/Q$ vs $v^{1/2}$ plot, which, in our experience, is frequently nonlinear. In fact, the quantity of charge associated with reaction 1 should increase by lowering the scan rate until a maximum value is obtained, which corresponds to the total number of sites available. The extrapolation for $v^{1/2} \rightarrow 0$ provides the better estimation of Q_{tot}.

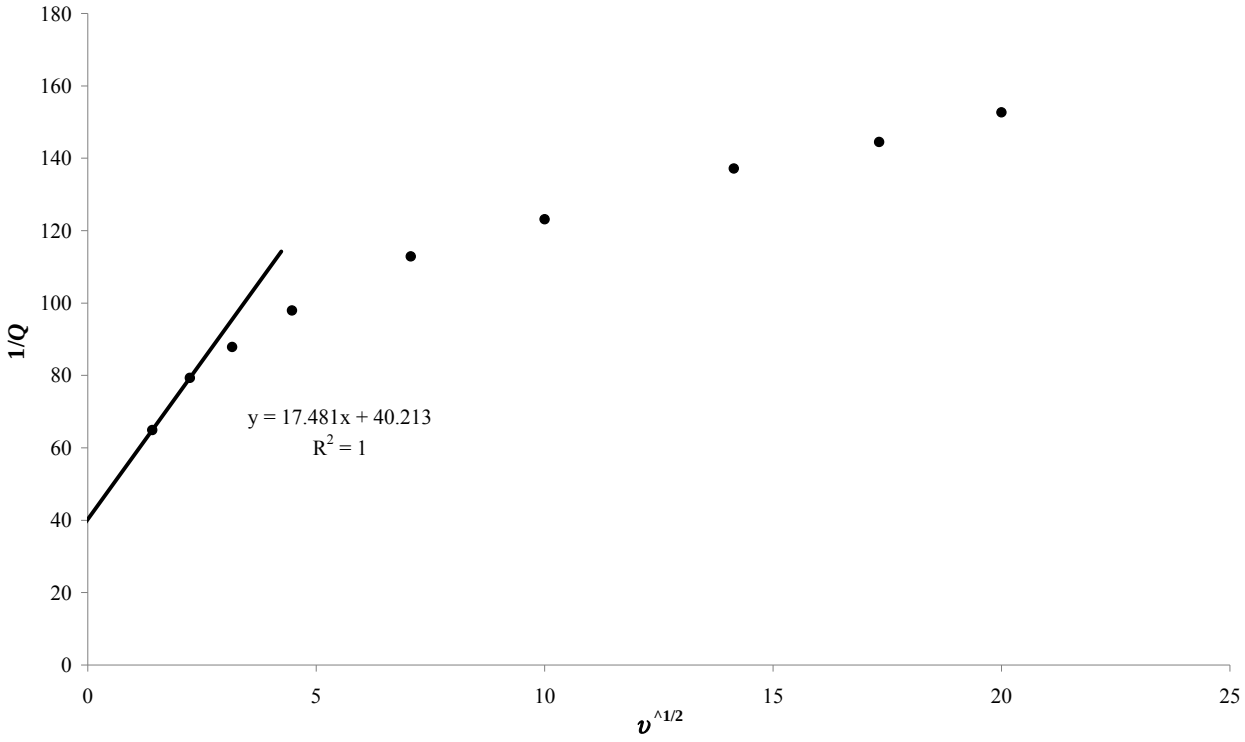

Figure S6. Example of extrapolation of Q to $v \rightarrow 0$, on the data represented in Figure S4 for the determination of Q_{tot}.

The ratio between Q_{out} and Q_{tot} should give a good estimation of the accessibility of active sites by protons. In the case of IrO_2 electrode, $Q_{out}/Q_{tot} \approx 0.6$-$0.7$, thus indicating that many sites are not rapidly accessible to protons. Moreover, a very small amount of sites were found to actually participate in reaction 7. The amount, estimated starting from the values of Q_{tot}, is about 1% of the total Ir atoms in 1 M $HClO_4$ or 1 M NaOH or 0.5% in neutral media. This agrees with the results shown in Ref. 14, in which the number of active sites was estimated to be 1% of their total. The discrepancy observed between neutral pHs and extreme pHs could be due, as suggested in reference 6, to the role of H^+ ions in reaction 1, as well as their slow diffusion to the sites. The low number of sites participating in reaction 7, as well as the low number of Q_{out}/Q_{tot}, suggests the possibility to design new materials containing low amounts of active (and expensive) material dispersed in a low cost, inert matrix.[15,16] In the case of composite IrO_2/MO_x electrodes (M being a second metal), Q_{out}/Q_{tot} ratios are generally higher, due to a better accessibility of the active sites with respect to the pure IrO_2 electrodes.[10,13,17] The sites actually participating in the pseudocapacitive phenomena is even lower for Co_3O_4, about 0.2%, and also in this case the ratio is around $Q_{out}/Q_{tot} \approx 0.7$ in PBS at pH 6.8 and 11.3 up to 0.9 in 1 M NaOH. This suggests that Co_3O_4 layers are more compact than

IrO_2 ones, thus reducing the electrochemical porosity and the number of sites involved in the solid state redox transition.

Additional i-E curves of Co-Pi layers on FTO or Ni substrates

As shown in Figure S7 and compared with Figures 15 and 16, the substrate (FTO or Ni) seems not to be a key factor to affect the voltammetric behavior, rather the film preparation conditions, such as the potential and rate for electrodeposition are important.

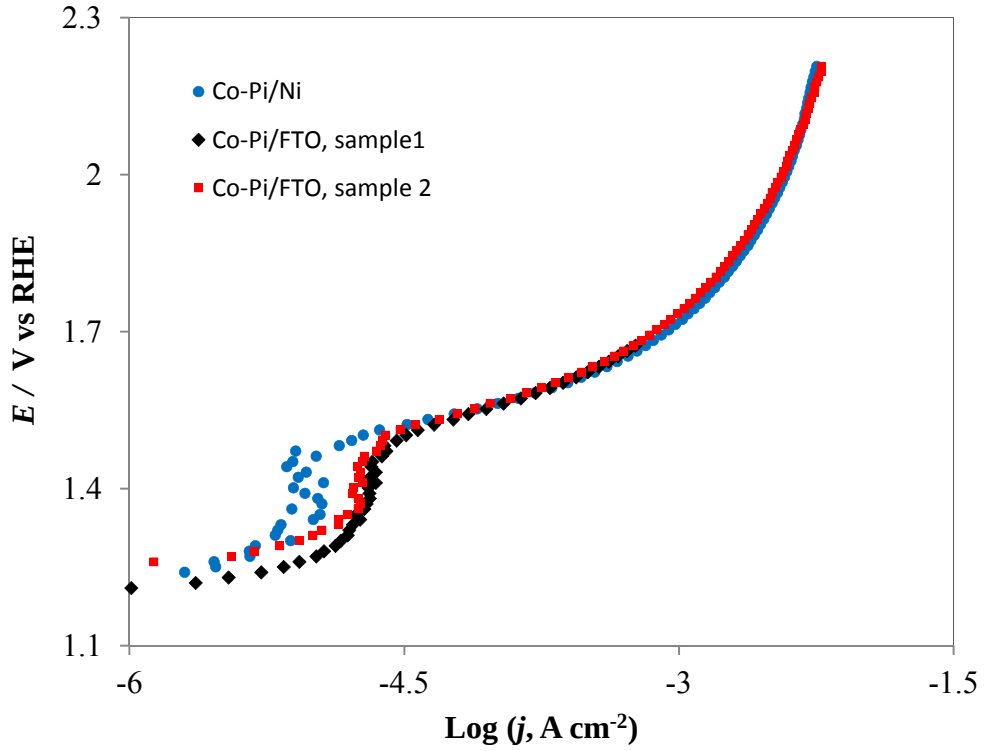

Figure S7. Polarization curves in a stirring 0.1 M PBS (pH 6.8) at a scan rate of 0.0001 V/s. Blue circles on Ni; Black diamonds on FTO sample 1; Red squares on FTO sample 2. Electrodeposition conditions: Constant potential at 0.85 V vs Ag/AgCl. Solution is quiet without dearation during deposition. Anodic charge collected = 0.35 C for overnight (16 – 17 hrs.)

Stability of IrO_2 electrodes under strong alkaline conditions

Iridium oxide is known to be active under alkaline conditions. However, there are evidences of its limited stability, likely due to the formation of iridates (see the main text).

To prove the reliability of the polarization curves recorded on the IrO_2 electrode at pH 14.0, the following voltammetric curves were recorded before and after the polarization curve recording. The main difference in the two curves is due to the presence of different faradic currents relevant to the oxygen reduction reaction, that occurs at potentials less positive than 0.6 V (Ag/AgCl). The

differences are therefore due to different amounts of oxygen dissolved in the solution (that was not degassed before the CVs) before and after the polarization curve recorded under OER conditions. The potential window in which the oxygen reduction does not occur (0.2-0.6 V vs Ag/AgCl) are almost completely overlapped, thus proving that the material was not degradated.

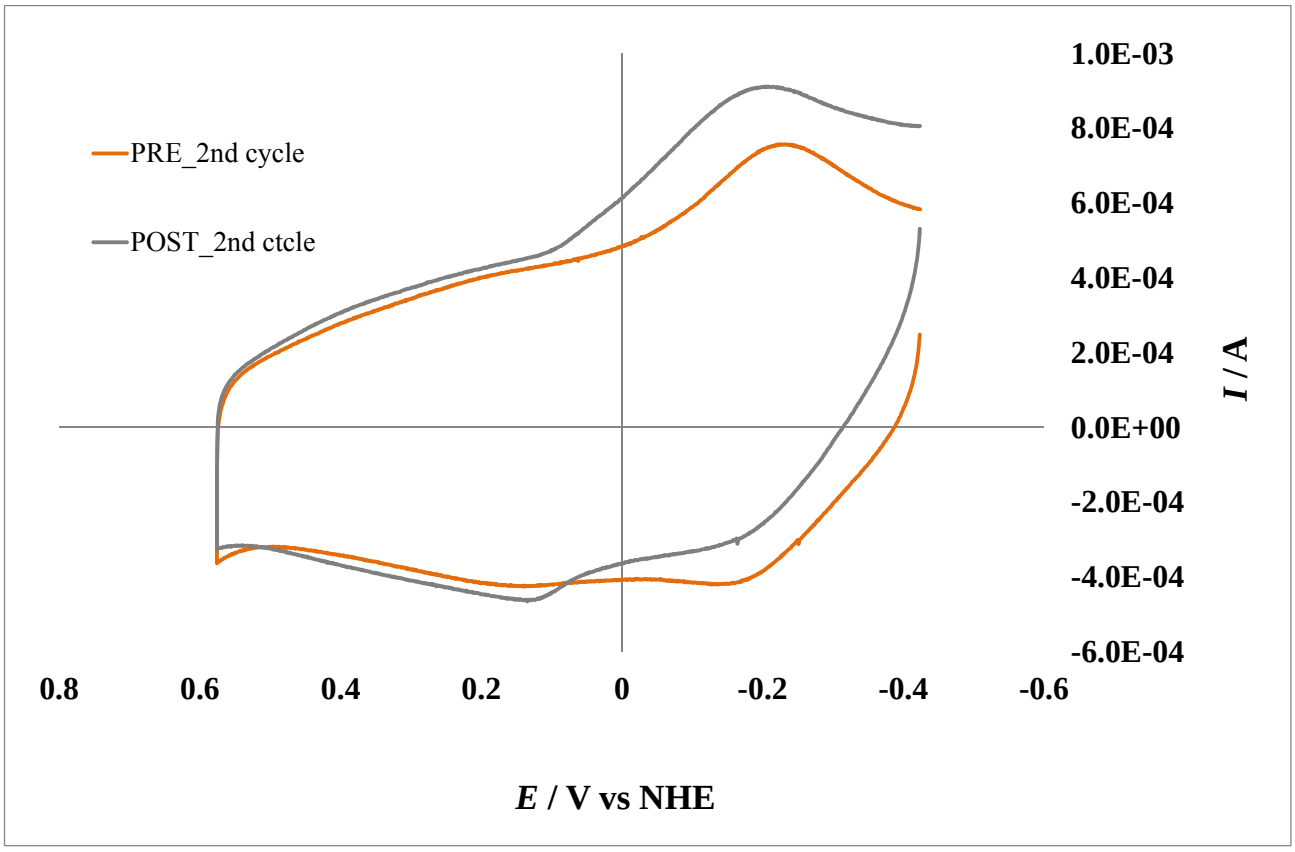

Figure S8. CV recorded on an IrO_2 electrode in 1M NaOH (pH = 14.0): before (orange line) and after (grey line) the recording of the polarization curve reported in the main text.

References

[1] C. P. De Pauli and S. Trasatti, *J. Electroanal. Chem.,* 1995, **396**, 161.
[2] S. Ardizzone, A. Carugati and S. Trasatti, *J. Electroanal. Chem.,* 1981**,** **126**, 287.
[3] L. Ouattara, S. Fierro, O. Frey, M. Koudelka and C. Comninellis, *J. Appl. Electrochem.,* 2009, **39**, 1361.
[4] R. Boggio, A. Carugati and S. Trasatti, *J. Appl. Electrochem.,* 1987, **17**, 828.
[5] G. Spinolo, S. Ardizzone, and S. Trasatti, *J. Electroanal. Chem.* 1997, **423**, 49.
[6] M. Pourbaix, *Atlas of Electrochemical Equilibria in Aqueous Solutions*., National Association of Corrosion Engineers: Houston, Texas, 2nd. English ed., 1974.
[7] S. Ardizzone, G. Fregonara, and S. Trasatti, *Electrochim. Acta,* 1990, **35**, 263-267.
[8] K. Doblhofer, M. Metikos, Z. Ogumi and H. Gerischer, *Ber. Bunsenges. Phys. Chem.,* 1978, **85**, 1046.
[9] G. Spinolo, S. Ardizzone and S. Trasatti, *J. Electroanal. Chem.,* 1997, **423**, 49.

[10] C. P. De Pauli and S.Trasatti, *J. Electroanal. Chem*., 2002, **145**, 538-539.
[11] S. Fierro, L. Ouattara, E. H. Calderon, and C. Comninellis, *Electrochem. Comm.,* 2008, **10**, 955.
[12] W. Sugimoto, T. Kizaki, K. Yokoshima, Y. Murakami and Y. Takasu, *Electrochim. Acta,* 2004**, 49**, 313.
[13] S. Ardizzone, C. L. Bianchi, L. Borgese, G. Cappelletti, C. Locatelli, A. Minguzzi, S. Rondinini A. Vertova, P. C. Ricci, C. Cannas and A. Musinu, *J. Appl. Electrochem.*, 2009, **39**, 2039.
[14] S. Fierro, T. Nagel, H. Baltruschat, and C. Comninellis, *Electrochem. Comm.,* 2007, **9**, 1969.
[15] A. Minguzzi, M. A. Alpuche-Aviles, J. Rodríguez López, S. Rondinini and A. J. Bard, *Anal. Chem*., 2008, **80**, 4055.
[16] S. Ardizzone, C. L. Bianchi, G. Cappelletti, M. Ionita, A. Minguzzi, S. Rondinini and A. Vertova, *J. Electroanal. Chem.,* 2006, **589**, 160.
[17] L. Vazquez-Gomez, S. Fierro and A. De Battisti, *Appl. Cat. B.,* 2006, **67**, 34.